RESTORATION-BASED IRON OXIDE PARTICLES QUANTIFICATION IN MR IMAGES

Delphine Charpigny, Thomas Grenier, Christophe Odet, Hugues Benoit-Cattin

CREATIS, INSA de lyon, Université de Lyon,
CNRS UMR 5220, Inserm U 630, 69621 Villeurbanne, France

ABSTRACT

Magnetic Resonance Imaging (MRI) is a medical imaging modality that provides structural and functional information. To improve the contrast of MR images, contrast agents, such as Ultrasmall SuperParamagnetic Iron Oxide particles (USPIO), are more commonly being used. Quantifying and locating these nanoparticles is of high interest. An efficient technique consists in images analyzing of the default field inhomogeneities induced by USPIOs. In a previous work, we have introduced such a quantification framework. Here, we improve our approach by deriving from two methods: Wiener and CLS filtering. Both methods have been evaluated on realistic data demonstrating that CLS filtering gives very promising quantification results.

Index Terms— Filter Noise, image restoration, quantification, molecular MRI, magnetic susceptibility

1. INTRODUCTION

Magnetic Resonance Imaging (MRI) is a relative contrast-measurement technique in medical imaging [1]. It allows one to visualise structure and function of the body. In recent years, contrast agents are more commonly being used for improving the observed contrast, for diagnosis or for cell tracking. Contrast agents are of two kinds: positive contrast agents and negative contrast agents. Whereas positive contrast agents appear as bright spots in the image, negative contrast agents, such as Ultrasmall SuperParamagnetic Iron Oxide particles (USPIOs), produce signal voids. Quantifying and locating USPIOs is a fundamental non-trivial problem in molecular MR imaging [2].

Many techniques have been developed to quantify contrast agents, and USPIOs more specifically. As the magnetic susceptibility of USPIOs is linked to their concentration [3], analysing USPIOs susceptibility effect on the MR images is of high interest. Contrast-measurement techniques, such as T_2^* (or T_2) cartography or positive contrast techniques with negative contrast agents [4] have been considered. Another strategy consists in studying the magnetic field inhomogeneities [5, 6]. Indeed, USPIOs have a magnetic susceptibility different from the surrounding media, and this difference produces magnetic field inhomogeneities, also called default field.

In this paper, we propose to model the iron oxide particles quantification problem as a restoration problem. First, we will detail the proposed quantification framework with restoration methods, from the method used to analyze field inhomogeneities, to noise considerations. Secondly, we propose to derive our approach with two methods of restoration: the Wiener-Fourier filter and the Constrained Least Squares (CLS) filter. Finally, a comparison between these two methods has been made and applied on realistic synthetic images.

2. USPIOS QUANTIFICATION FRAMEWORK

Fig. 1 presents our USPIOs quantification framework with restoration methods.

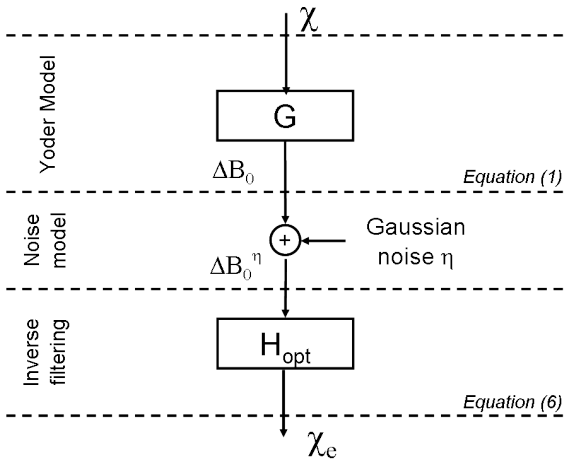

Fig. 1. Restoration-based quantification framework overview.

It starts by linking the magnetic susceptibility to the magnetic field inhomogeneities through the linear filter G described in section 2.1. The obtained default field map ΔB_0 is perturbed by Gaussian additive noise. The deconvolution process is performed in the Fourier domain to retrieve the magnetic susceptibility χ_e. Section 2.2 presents the initial solution that is based on the inverse filter of G. And, section 2.3 illustrates the noise effect in the deconvolution process.

2.1. Magnetic field inhomogeneities model

Yoder *et al.* [7] mathematically describe the magnetic field inhomogeneities, called default field ΔB_0, as follows:

$$\Delta B_0(\mathbf{v}) = \frac{B_0}{3}\chi(\mathbf{v}) + \frac{B_0}{4\pi}(\Delta\chi \otimes D)(\mathbf{v}) \quad (1)$$

where χ is the magnetic susceptibility, $\Delta\chi$ the gradient of the function χ (calculated in the direction of the main field B_0), B_0 the intensity of the main field, and $\otimes$ the convolution product. D is a convolution kernel defined by:

$$D(\mathbf{v}) = \oint_{S_k} \frac{z'-z}{|\mathbf{v}'-\mathbf{v}|^3}\,\mathbf{B_0}\mathbf{dS}' \quad (2)$$

where $\mathbf{v} = (x, y, z)$ is the position vector where the kernel is calculated, $\mathbf{v}' = (x', y', z')$ is a voxel of the closed surface S_k. Equation (1) can be written as follows:

$$\Delta B_0 = \chi \otimes G \quad (3)$$

As an illustration, Fig. 2(b) represents the profile of the default field ΔB_0 obtained by equation (1) from the susceptibility profile presented in Fig. 2(a).

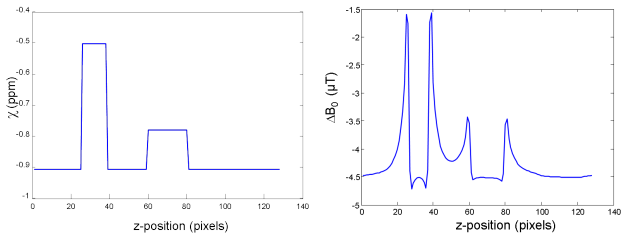

(a) χ (b) ΔB_0

Fig. 2. Profile of the default field induced by 2 spheres (closed in distance): $\chi_1 = -5\ ppm$ and $\chi_2 = -8\ ppm$. The main field B_0 has an intensity of 1.5 T.

2.2. Inverse filtering

In [6], we have introduced the inverse filter of G to perform the deconvolution in the Fourier domain. The estimated magnetic susceptibility χ_e is obtained in the Fourier domain by:

$$\widehat{\chi}_e(\mathbf{f}) = \Delta\widehat{B}_0(\mathbf{f}) \cdot \widehat{H}(\mathbf{f}) \quad (4)$$

The filter H has a transfer function $\widehat{H}(\mathbf{f})$ defined by:

$$\widehat{H}(\mathbf{f}) = \frac{1}{G} = \frac{1}{\frac{B_0}{3} + \frac{B_0}{4\pi}\left(\exp\left(2i\pi\frac{f_z}{N}\right) - 1\right)\widehat{D}(\mathbf{f})} \quad (5)$$

where $\mathbf{f} = (f_x, f_y, f_z)$ describes the position in the Fourier domain, N the number of pixels in the direction of B_0 and $\widehat{\cdot}$ denotes the Fourier transform.

2.3. Noise issues

In the restoration-based quantification framework (fig. 1), we make the assumption that Gaussian white noise $\eta(\sigma_n)$ is added to the default field map ΔB_0 [8]. It is well known that direct deconvolution is highly sensitive to noise, as illustrated in Fig. 3.

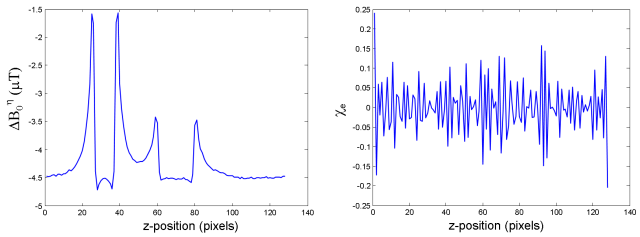

(a) ΔB_0^{η} (b) χ_e

Fig. 3. Inverse filtering result 3(b) from noisy default field 3(a) ($\sigma_n = 10^{-2}$). $\Delta B_0^{\eta} = \Delta B_0 + \eta$.

Fig. 3 presents the estimated magnetic susceptibility χ_e (fig. 3(b)) obtained from a noisy default field map (fig. 3(a)). The deconvolution fails, and we can not retrieve the profile of the magnetic susceptibility χ presented in fig. 2(a), χ_e is useless. Restoration methods have to be considered.

3. RESTORATION METHODS APPLIED TO USPIOS QUANTIFICATION

To improve the robustness of the deconvolution in presence of noise, we considered restoration techniques to design the inverse filter H_{opt} based on H. Equation (4) becomes:

$$\widehat{\chi}_e(\mathbf{f}) = \Delta\widehat{B}_0(\mathbf{f}) \cdot \widehat{H}_{\text{opt}}(\mathbf{f}) \quad (6)$$

where $\widehat{H}_{\text{opt}}(\mathbf{f})$ denotes a transfer function associated to a restoration method. In this paper, two approaches are compared: Wiener-Fourier filtering and Constrained Least Squares filtering [9].

3.1. Wiener-based quantifcation

The Wiener-Fourier filter aims to minimize the mean square error between the uncorrupted volume χ and the estimated volume χ_e. We replace, in equation (6), $\widehat{H}_{\text{opt}}(\mathbf{f})$ by $\widehat{H}_{\text{W}}(\mathbf{f})$ defined by:

$$\widehat{\text{H}}_{\text{w}}(\mathbf{f}) = \frac{\left|\frac{1}{\widehat{\text{H}}(\mathbf{f})}\right|^2}{\left|\frac{1}{\widehat{\text{H}}(\mathbf{f})}\right|^2 + \text{K}} \cdot \widehat{\text{H}}(\mathbf{f}) \quad (7)$$

where, K is a tuning parameter related to noise.
From equations (6) and (7), equation (6) becomes:

$$\widehat{\chi}_e(\mathbf{f}) = \frac{\left|\frac{1}{\widehat{\mathrm{H}}(\mathbf{f})}\right|^2}{\left|\frac{1}{\widehat{\mathrm{H}}(\mathbf{f})}\right|^2 + \mathrm{K}} \cdot \widehat{\mathrm{H}}(\mathbf{f}) \cdot \Delta \mathrm{B}_0 \tag{8}$$

3.2. CLS-based quantifcation

The Constrained Least Squares (CLS) filter, defined in equation (9), is an optimisation of the Wiener-Fourier filter. We replace, in equation (6), H_{opt} by H_{CLS} defined by:

$$\widehat{\mathrm{H}}_{\mathrm{CLS}}(\mathbf{f}) = \frac{\left|\frac{1}{\widehat{\mathrm{H}}(\mathbf{f})}\right|^2}{\left|\frac{1}{\widehat{\mathrm{H}}(\mathbf{f})}\right|^2 + \mathrm{K}\left|\widehat{\mathrm{P}}(\mathbf{f})\right|^2} \cdot \widehat{\mathrm{H}}(\mathbf{f}) \tag{9}$$

where $\widehat{P}$ is the Fourier transform of a 3D Laplacian operator defined in equation (10) and K a parameter to adjust so that the noise is reduced. After investigations, we design, in the spatial domain, the Laplacian operator as a 3x3x3 matrix by:

$$\begin{aligned} &\forall (i,j,k) \in \{-1\ ;\ 0\ ;\ 1\} \\ &P(i,j,k) = \begin{cases} 26 \text{ if } \mathrm{i=j=k=0} \\ -1 \text{ otherwise} \end{cases} \end{aligned} \tag{10}$$

From equations (6) and (9), equation (6) becomes:

$$\widehat{\chi}_e(\mathbf{f}) = \frac{\left|\frac{1}{\widehat{\mathrm{H}}(\mathbf{f})}\right|^2}{\left|\frac{1}{\widehat{\mathrm{H}}(\mathbf{f})}\right|^2 + \mathrm{K}\left|\mathrm{P}(\mathbf{f})\right|^2} \cdot \widehat{\mathrm{H}}(\mathbf{f}) \cdot \Delta \mathrm{B}_0 \tag{11}$$

The results using Wiener-Fourier filtering and CLS filtering are compared in the next section.

4. EVALUATION

4.1. Materials

Evaluation has been conducted on a χ-volume presented in Fig.4(a). This model is composed of 4 classes that describe an inflamed artery labelled with USPIOs [10]. The table 1 presents the susceptibility value for each label. Fig. 4(b) presents the induced default feld for $B_0 = 1T$.

class	0	1	2	3
χ (ppm)	-9.05	1.8	16.8	32.2

Table 1. Susceptibility values associated to label.

We add to the ΔB_0 volume (presented fig. 4(b)), Gaussian white noise characterised by its normalised standard deviation $\sigma_n = \sigma_{\text{noise}}/\mu_{\Delta \mathrm{B}_0}$, where $\mu_{\Delta B_0}$ is the mean of ΔB_0.

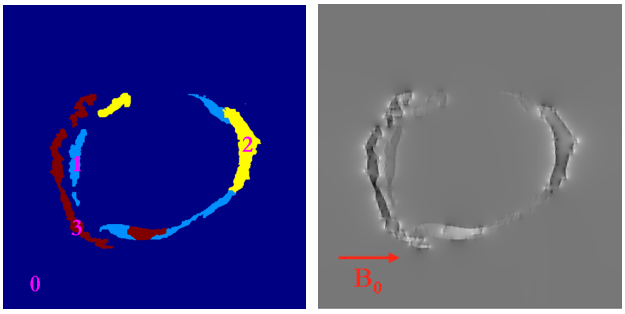

(a) χ volume (b) ΔB_0 volume

Fig. 4. Middle-slice of: (a) the test volume - (b) the default field computed from the test volume with equation (1).

We study the contribution of restoration methods for realistic noise ($10^{-2} < \sigma_n < 5.10^{-1}$).

4.2. Results

In this section, we present the comparison between the two restoration methods presented in section 3. To quantify the contribution of each approach, the Peak Signal to Noise Ratio (PSNR) has been investigated. We calculate the PSNR (in dB) as follows:

$$\mathrm{PSNR} = 10 \log_{10}\left(\frac{|\max(\chi)|^2}{MSE}\right) \tag{12}$$

where MSE is the Mean Square Error between the estimated χ_e and the uncorrupted χ and defined by:

$$MSE = \frac{1}{C}\sum(\chi - \chi_e)^2 \tag{13}$$

where C denotes the pixels number of the volume.

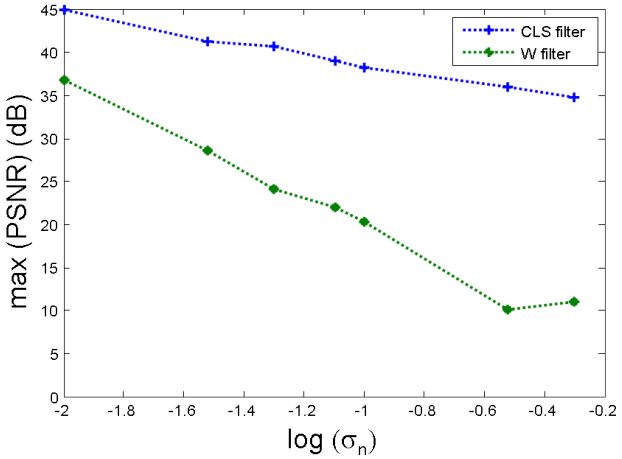

Fig. 5. Evolution of the max of the PSNR with increasing σ_n with the Wiener (green plot) and the CLS (blue plot) filter.

Fig. 5 presents the evolution of the maximum of the PSNR with increasing noise. For each point of the plot, we have search the maximum of the PSNR with the Wiener (resp. CLS) filter in respect to the tuning parameter K for different values of σ_n (from $\sigma_n = 10^{-2}$ to $\sigma_n = 5.10^{-1}$). Regarding Fig. 5, it appears that in any case CLS filter gives a better PSNR than Wiener filter, for an appropriate choice of the tuning parameter. For $\sigma_n = 0.1$, the PSNR is equal to 6 dB without restoration methods. It rises to 20.3 dB with the Wiener filter and to 38.2 dB with the CLS.

Fig. 6 presents the normalised error maps, defined by equation (14), between the uncorrupted volume χ and the estimated volume χ_e obtained with Wiener filter (Fig. 6(a)) and CLS filter (Fig. 6(b)).

$$error = \left| \frac{\chi - \chi_e}{\chi} \right| \tag{14}$$

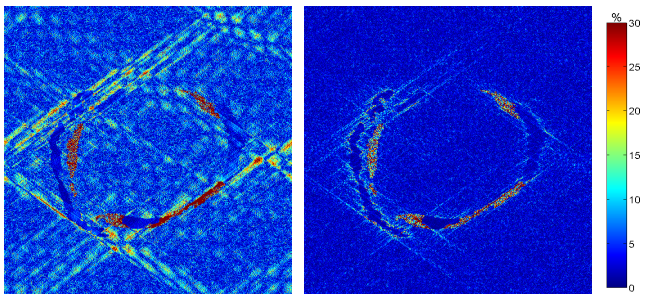

(a) Wiener-based quantification (b) CLS-based quantification

Fig. 6. Error map between the uncorrupted χ presented fig. 4(a) and the estimated χ_e obtained with: (a) Wiener filter - (b) CLS filter at a noise level of $\sigma_n = 10^{-2}$.

The mean squared error is equal to $1.6\ 10^{-11}$ with Wiener filtering, whereas with CLS filtering, the MSE is equal to $1.2\ 10^{-13}$. Fig. 6 confirms that CLS approach offers a better restoration of a complex and realistic object. The higher error is located on the borders of the classes that describe the object.

5. CONCLUSION

We propose a restoration-based quantification framework for iron oxide nanoparticles that has been tested on realistic synthetic data. CLS filtering appears to be more efficient than Wiener filtering and allows one to retrieve suceptibility map from a noisy default field information. Such framework does not rely on any acquisition parameters (such as TR, TE ...) or on the MRI sequence. Indeed, we only need default field maps that can be obtained from two gradient echo images (or volumes) [11] or by the recent susceptibility gradient map technique [12]. Based on the proposed framework restoration methods including a priori are under consideration to improve the robustness to noise.

6. REFERENCES

[1] P.C. Lauterbur, "Image formation by induced interaction: examples employing nuclear magnetic resonance," *nature*, vol. 242, pp. 190–191, 1973.

[2] E.M. Shapiro et al, "MRI detection of single particles for cellular imaging," *PNAS*, vol. 101(30), pp. 10901–10906, 2004.

[3] J.F. Schenk, "The role of magnetic susceptibility in magnetic resonance imaging: MRI magnetic compatibility of the first and second kinds," *Medical Physics*, vol. 23(6), pp. 815–850, 1996.

[4] C.H. Cunningham et al, "Positive contrast magnetic resonance imaging of cells labeled with magnetic nanoparticles," *Magnetic Resonance in Medicine*, vol. 53, pp. 99–1005, 2005.

[5] E.M. Haacke et al., "Imaging iron stores in the brain using magnetic resonance imaging," *Magnetic Resonance Imaging*, vol. 23, pp. 1–25, 2005.

[6] D. Charpigny et al., "Deconvolution approach for susceptibility map building," in *European Society for Magnetic Resonance in Medicine and Biology*, 2008, vol. in press.

[7] D.A. Yoder et al., "MRI simulator with static field inhomogeneities," in *Medical Imaging Proceedings*. SPIE, 2002, vol. 4684, pp. 592–603.

[8] D.G. Nishimura, *Principles of magnetic resonance imaging*, Stanford University, 1996.

[9] R.C. Gonzalez and R.E. Woods, *Digital Image Processing*, Prentice Hill, 3rd edition, 2008.

[10] O. Addy, D. Charpigny, M. Sigovan, E. Canet-Soulas, H. Benoit-Cattin, and D. Nishimura, "Mri simulation framework for atherosclerosis inflammation with uspios," in *Proc. EMIM 2009: 4th European Society for Molecular Imaging*, 2009.

[11] S. Kanayama et al., "In vivo rapid magnetic field measurement and shimming using single scan differential phase mapping," *Magnetic Resonance in Medicine*, vol. 36, pp. 637–642, 1996.

[12] H. Dahnke et al., "Susceptibility gradient mapping (SGM: a new method for positive contrast generation applied to superparamagnetic iron oxide particle (SPIO)-labeled cells," *Magnetic Resonance in Medicine*, vol. 60, pp. 595–603, 2008.